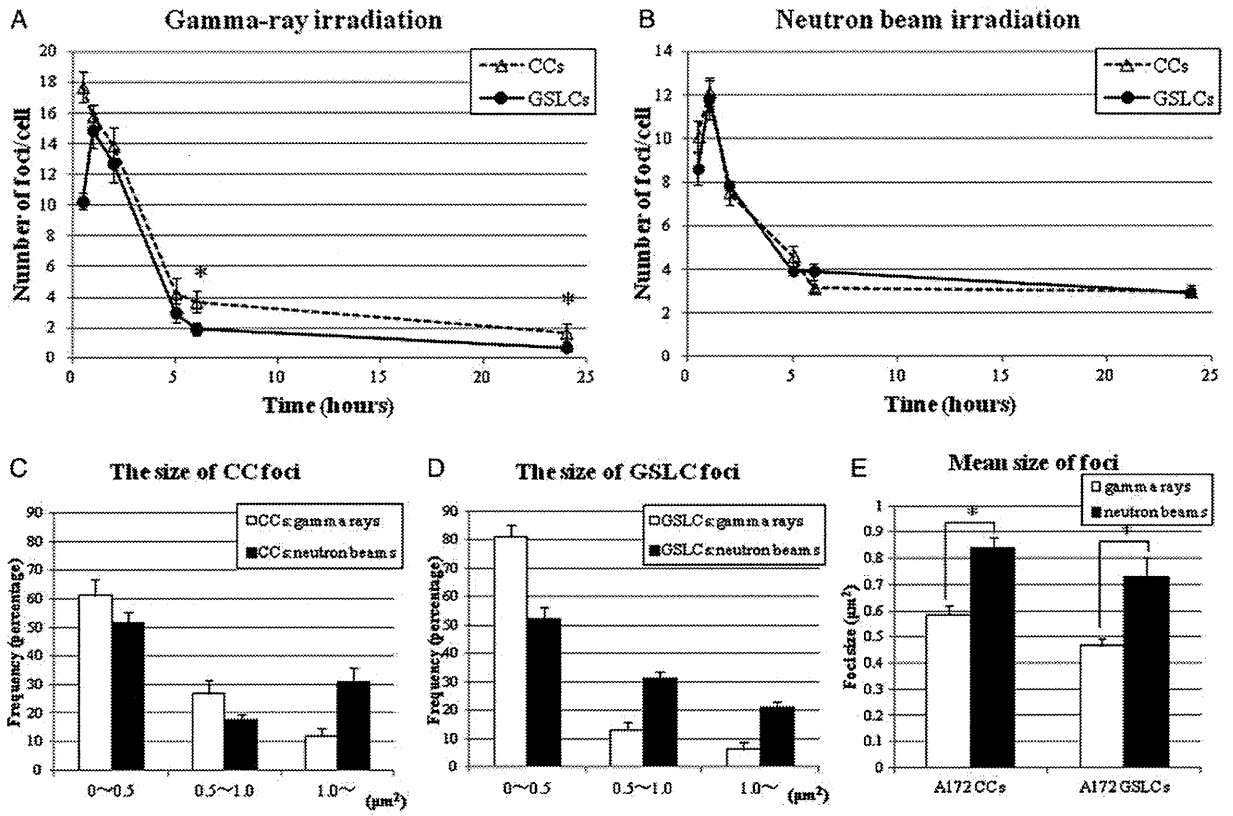

Fig. 4. Change in the number of induced nuclear gamma-H2AX foci and the histograms of gamma-H2AX foci size, at the times indicated post-irradiation in A172. These cells were irradiated with different types of beams (total physical dose = 4 Gy). (**A**) and (**B**) The numbers of gamma-H2AX foci per cell of GSLCs and CCs in A172 after the different types of radiation. (**C**) and (**D**) Distribution of gamma-H2AX foci sizes for A172 at 24 h post-irradiation. (**E**) Mean gamma-H2AX foci size for each type of A172 cells at 24 h post-irradiation. Bars represent the standard errors. $*P < 0.05$ compared with gamma-H2AX foci per cell in GSLCs and CCs. GSLCs = glioma stem-like cells; CCs = control cells.

in GSLCs. In fact, it has been reported that to evaluate gamma-H2AX foci in cells exposed to high-LET radiation, the size of the foci should be considered, since high-LET radiation can cause larger gamma-H2AX foci than low-LET radiation [11, 27]. We therefore investigated not only the numbers of foci but also their size after 24 h irradiation by both types of radiation, and found that high-LET radiation could cause larger gamma-H2AX foci than low-LET radiation in both GSLCs and CCs (Figs. 3, 4C, 4D and 4E). As Fig. 4E shows, high-LET radiation led to significantly larger gamma-H2AX foci than low-LET radiation did, in both GSLCs and CCs. Therefore, it is thought that high-LET radiation could cause more serious DNA DSBs than low-LET radiation, even in GSLCs. In the previous report [28], low-LET irradiation might produce relatively large foci with time. In our experiment we demonstrated that high-LET particles produce larger foci in GSLC than low-LET gamma rays.

Indeed, under both gamma-ray and neutron-beam irradiation, more than half of all gamma-H2AX foci were small (0–0.5 μm^2). It is speculated that the neutron beams from KUR formed a wide-range beam that included gamma rays and secondary gamma rays. At the absorbed dose of 4 Gy, the compositions of fast, epithermal and thermal neutrons as well as of gamma rays were 25.5%, 2.5%, 22% and 50%, respectively. Almost half of the neutron beam components of the absorbed dose were induced by gamma rays, which could explain why small foci were induced mainly by gamma rays, even under neutron-beam irradiation. As described above, Fig. 3 also shows that the fluorescence intensity of gamma-H2AX foci after neutron irradiation was higher than that after gamma-ray irradiation. This may explain why high-LET radiation causes more intense DNA damage than low-LET radiation. A previous study showed that high-LET radiation, such as that from heavy ion therapy, had several potential advantages over low-LET radiation due to its induction of complex DNA damage that was not easily repaired [29], and may have an advantage over low-LET radiation for cancer stem-like cells [30]. Thus, our data also support the potential for use of high-LET radiation for GSCs.

Heavy ion treatment and BNCT are recognized as forms of high-LET radiation. In a previous report, when chemo-irradiation was combined with carbon ion therapy, the median survival time of GBM patients was 17 months [31]. In another report, BNCT followed by X-ray radiation therapy led to a median survival time of GBM patients of 21.3 months, even without chemotherapy [9]. Although both of these reports involved small numbers of patients, the results suggested that, since these high-LET radiations were effective even for GSCs in a clinical setting, patients could show prolonged survival. At the moment these treatment modalities are still at the clinical trial stage, but they may improve the standard treatment for GBM.

Although various treatments for GBM have been tried, an unfavorable prognosis can be expected with the current standard treatment. In the present study, we demonstrated that high-LET radiation may be able to overcome GSC resistance to low-LET radiation. It is necessary to further investigate the usefulness of high-LET radiation for the control of GSCs. High-LET radiation therapies such as BNCT or heavy ion therapy have very important roles in further treatment for therapy-resistant GBM.

CONFLICT OF INTEREST

The authors have no conflicts of interest to disclose.

FUNDING

This work was supported by a Grant-in-Aid for Scientific Research (B) (23390355) from the Japanese Ministry of Education, Culture, Sports, Science and Technology to S-IM.

REFERENCES

1. Stupp R, Mason WP, van den Bent MJ *et al.* Radiotherapy plus concomitant and adjuvant temozolomide for glioblastoma. *N Engl J Med* 2005;**352**:987–96.
2. Singh SK, Clarke ID, Terasaki M *et al.* Identification of a cancer stem cell in human brain tumors. *Cancer Res* 2003;**63**: 5821–8.
3. Singh SK, Hawkins C, Clarke ID *et al.* Identification of human brain tumour initiating cells. *Nature* 2004;**432**:396–401.
4. Yuan X, Curtin J, Xiong Y *et al.* Isolation of cancer stem cells from adult glioblastoma multiforme. *Oncogene* 2004;**23**: 9392–400.
5. Bao S, Wu Q, McLendon RE *et al.* Glioma stem cells promote radioresistance by preferential activation of the DNA damage response. *Nature* 2006;444:756–60.
6. Chang CJ, Hsu CC, Yung MC *et al.* Enhanced radiosensitivity and radiation-induced apoptosis in glioma CD133-positive cells by knockdown of SirT1 expression. *Biochem Biophys Res Commun* 2009;**380**:236–42.
7. Miyatake S, Kawabata S, Kajimoto Y *et al.* Modified boron neutron capture therapy for malignant gliomas performed using epithermal neutron and two boron compounds with different accumulation mechanisms: an efficacy study based on findings on neuroimages. *J Neurosurg* 2005;**103**:1000–9.
8. Miyatake S, Tamura Y, Kawabata S *et al.* Boron neutron capture therapy for malignant tumors related to meningiomas. *Neurosurgery* 2007;**61**:82–90; discussion 90–1.
9. Kawabata S, Miyatake S, Kuroiwa T *et al.* Boron neutron capture therapy for newly diagnosed glioblastoma. *J Radiat Res* 2009;**50**:51–60.
10. Miyatake S, Kawabata S, Yokoyama K *et al.* Survival benefit of Boron neutron capture therapy for recurrent malignant gliomas. *J Neurooncol* 2009;**91**:199–206.
11. Kinashi Y, Takahashi S, Kashino G *et al.* DNA double-strand break induction in Ku80-deficient CHO cells following boron neutron capture reaction. *Radiat Oncol* 2011;**6**:106.
12. Qiang L, Yang Y, Ma YJ *et al.* Isolation and characterization of cancer stem like cells in human glioblastoma cell lines. *Cancer Lett* 2009;**279**:13–21.
13. Sakurai Y, Kobayashi T. Characteristics of the KUR Heavy Water Neutron Irradiation Facility as a neutron field with variable energy spectra. *Nucl Instrum Meth A* 2000;**453**:569–96.
14. Kobayashi T, Kanda K. Analytical calculation of boron-10 dosage in cell nucleus for neutron capture therapy. *Radiat Res* 1982;**91**:77–94.
15. Kitao K. A method for calculating the absorbed dose near interface from 10B(n, alpha)7Li reaction. *Radiat Res* 1975; **61**:304–15.
16. Ohnishi T, Mori E, Takahashi A. DNA double-strand breaks: their production, recognition, and repair in eukaryotes. *Mutat Res* 2009;**669**:8–12.
17. Fukaya R, Ohta S, Yamaguchi M *et al.* Isolation of cancer stem-like cells from a side population of a human glioblastoma cell line, SK-MG-1. *Cancer Lett* 2010;**291**:150–7.
18. Vescovi AL, Galli R, Reynolds BA. Brain tumour stem cells. *Nat Rev Cancer* 2006;**6**:425–36.
19. Baumann M, Krause M, Hill R. Exploring the role of cancer stem cells in radioresistance. *Nat Rev Cancer* 2008;**8**:545–54.
20. Baumann M, Krause M, Thames H *et al.* Cancer stem cells and radiotherapy. *Int J Radiat Biol* 2009;**85**:391–402.
21. Ogden AT, Waziri AE, Lochhead RA *et al.* Identification of A2B5+CD133– tumor-initiating cells in adult human gliomas. *Neurosurgery* 2008;**62**:505–14; pdiscussion 514–5.
22. Shimura T, Noma N, Oikawa T *et al.* Activation of the AKT/cyclin D1/Cdk4 survival signaling pathway in radioresistant cancer stem cells. *Oncogenesis* 2012;**1**:e12.
23. van Gent DC, Hoeijmakers JH, Kanaar R. Chromosomal stability and the DNA double-stranded break connection. *Nat Rev Genet* 2001;**2**:196–206.
24. Leatherbarrow EL, Harper JV, Cucinotta FA *et al.* Induction and quantification of gamma-H2AX foci following low and high LET-irradiation. *Int J Radiat Biol* 2006;**82**:111–8.
25. Schmid TE, Dollinger G, Beisker W *et al.* Differences in the kinetics of gamma-H2AX fluorescence decay after exposure to low and high LET radiation. *Int J Radiat Biol* 2010;**86**: 682–91.
26. Prevo R, Deutsch E, Sampson O *et al.* Class I PI3 kinase inhibition by the pyridinylfuranopyrimidine inhibitor PI-103 enhances tumor radiosensitivity. *Cancer Res* 2008;**68**:5915–23.
27. Ibanez IL, Bracalente C, Molinari BL *et al.* Induction and rejoining of DNA double strand breaks assessed by H2AX

phosphorylation in melanoma cells irradiated with proton and lithium beams. *Int J Radiat Oncol Biol Phys* 2009;**74**: 1226–35.

28. Yamauchi M, Oka Y, Yamamoto M *et al.* Growth of persistent foci of DNA damage checkpoint factors is essential for amplification of G1 checkpoint signaling. *DNA Repair (Amst)* 2008; **7**:405–17.
29. Okayasu R, Okada M, Okabe A *et al.* Repair of DNA damage induced by accelerated heavy ions in mammalian cells proficient and deficient in the non-homologous end-joining pathway. *Radiat Res* 2006;**165**:59–67.
30. Cui X, Oonishi K, Tsujii H *et al.* Effects of carbon ion beam on putative colon cancer stem cells and its comparison with X-rays. *Cancer Res* 2011;**71**:3676–87.
31. Mizoe JE, Tsujii H, Hasegawa A *et al.* Phase I/II clinical trial of carbon ion radiotherapy for malignant gliomas: combined X-ray radiotherapy, chemotherapy, and carbon ion radiotherapy. *Int J Radiat Oncol Biol Phys* 2007;**69**:390–6.

Hiramatsu et al. Radiation Oncology 2013, 8:192
http://www.ro-journal.com/content/8/1/192

RADIATION ONCOLOGY

RESEARCH Open Access

Identification of early and distinct glioblastoma response patterns treated by boron neutron capture therapy not predicted by standard radiographic assessment using functional diffusion map

Ryo Hiramatsu, Shinji Kawabata*, Motomasa Furuse, Shin-Ichi Miyatake and Toshihiko Kuroiwa

Abstract

Background: Radiologic response of brain tumors is traditionally assessed according to the Macdonald criteria 10 weeks from the start of therapy. Because glioblastoma (GB) responds in days rather than weeks after boron neutron capture therapy (BNCT) that is a form of tumor-selective particle radiation, it is inconvenient to use the Macdonald criteria to assess the therapeutic efficacy of BNCT by gadolinium-magnetic resonance imaging (Gd-MRI). Our study assessed the utility of functional diffusion map (fDM) for evaluating response patterns in GB treated by BNCT.

Methods: The fDM is an image assessment using time-dependent changes of apparent diffusion coefficient (ADC) in tumors on a voxel-by-voxel approach. Other than time-dependent changes of ADC, fDM can automatically assess minimum/maximum ADC, Response Evaluation Criteria In Solid Tumors (RECIST), and the volume of enhanced lesions on Gd-MRI over time. We assessed 17 GB patients treated by BNCT using fDM. Additionally, in order to verify our results, we performed a histopathological examination using F98 rat glioma models.

Results: Only the volume of tumor with decreased ADC by fDM at 2 days after BNCT was a good predictor for GB patients treated by BNCT (P value = 0.022 by log-rank test and 0.033 by wilcoxon test). In a histopathological examination, brain sections of F98 rat glioma models treated by BNCT showed cell swelling of both the nuclei and the cytoplasm compared with untreated rat glioma models.

Conclusions: The fDM could identify response patterns in BNCT-treated GB earlier than a standard radiographic assessment. Early detection of treatment failure can allow a change or supplementation before tumor progression and might lead to an improvement of GB patients' prognosis.

Keywords: ADC, BNCT, Diffusion MRI, fDM, GB

Background

Surgery followed by radiation therapy is still the standard treatment for glioblastoma (GB). The addition of temozolomide (TMZ) chemotherapy to the standard treatment has significantly increased the proportion of patients who survive longer than 2 years [1]. However, additional progress is needed, as almost half of GB patients do not survive the first year after diagnosis.

Boron neutron capture therapy (BNCT) has been developed in the hope of achieving a breakthrough in GB treatment [2,3]. BNCT is a form of tumor-selective particle radiation therapy. We have applied BNCT to over 80 GB patients and have reported its survival benefit [4]. Additionally, a phase II multicenter clinical trial of BNCT is currently underway in Japan. In our substantial experience of clinical BNCT, we have frequently experienced dramatic reductions in enhanced lesion size on gadolinium-magnetic resonance imaging (Gd-MRI) obtained 2 to 7 days after BNCT [2,3]. Assessment of

* Correspondence: neu046@poh.osaka-med.ac.jp
Department of Neurosurgery, Osaka Medical College, 2-7 Daigaku-machi, Takatsuki City, Osaka 569-8686, Japan

BioMed Central

© 2013 Hiramatsu et al.; licensee BioMed Central Ltd. This is an Open Access article distributed under the terms of the Creative Commons Attribution License (http://creativecommons.org/licenses/by/2.0), which permits unrestricted use, distribution, and reproduction in any medium, provided the original work is properly cited.

radiation and chemotherapy efficacy for GB patients is traditionally accomplished by measuring changes in contrast enhancement of tumors at 10 weeks from the start of therapy using Gd-MRI, using the so-called Macdonald criteria [5]. The Macdonald criteria guide standard radiographic assessments, and have been correlated with survival [5-7]. However, because GB responds in days rather than weeks after BNCT, it is inconvenient to use the Macdonald criteria (including the conventional timing) to assess the therapeutic efficacy of BNCT by Gd-MRI.

On the other hand, the current standard treatment for GB patients, combined chemo-irradiation with TMZ, may induce pseudoprogression in 20–30% of cases [8], defined as an increase of contrast enhancement and/or edema on MRI without true tumor progression [9]. Also, full-blown radiation necrosis may be more frequent after combined chemo-irradiation. Pseudoresponse - namely, a decrease in contrast enhancement of brain tumors on MRI without a decrease of tumor activity - is frequent after treatment with vascular endothelial growth factor receptor signalling pathway inhibitors. Just as it is difficult to evaluate response patterns of GB treated by BNCT, so also cases with pseudoprogression, radiation necrosis, or pseudoresponse are difficult to assess using standard radiography because of changes in contrast enhancement that do not reflect tumor activity.

Diffusion MRI, which measures the random (Brownian) motion of water, has been proposed as an early biomarker for tumor response that does not rely on the measurement of contrast enhancement [10], and has been evaluated in preclinical [11,12] and clinical studies [13-15]. Diffusion MRI measurements are sensitive and can be used to detect and quantify tissue water diffusion values, which have been proposed to be related to the ratio of intracellular water to extracellular water; thus, changes in apparent diffusion coefficient (ADC) are inversely correlated with changes in cellularity. In this scenario, increases in ADC would reflect an increase in the mobility of water, either through the loss of membrane integrity or an increase in the proportion of total extracellular fluid with a corresponding decrease in cellular size or number, as seen with necrosis or apoptosis. In contrast, decreases in ADC reflect a decrease in free extracellular water, either through an increase in total cellular size or number, as can be seen with tumor progression or tumor cell swelling [16].

Functional diffusion map (fDM) was developed to take advantage of these principles on a voxel-by-voxel approach, and have proven to be a powerful tool for predicting the effect of chemotherapy and radiotherapy [10,15,17]. An increased ADC has been shown to correlate with a decrease in cellularity as a result of successful treatment [11,18] and/or radiation necrosis [18]. Other than time-dependent changes of ADC, fDM could automatically assess minimum (Min)/maximum (Max) ADC, Response Evaluation Criteria In Solid Tumors (RECIST), and the volume of enhanced lesions in response to BNCT over time.

In the current study, the usefulness of fDM as a predictive biomarker for GB patients treated with radiochemotherapy was reported [14,15]. There are no reports about the usefulness of fDM for GB treated by BNCT. In order to verify the usefulness of fDM for GB patients treated by BNCT, we assessed 17 GB patients treated by BNCT with fDM at 2 days after BNCT and examined a relationship between all the above factors analyzed by fDM (time-dependent changes of ADC, Min/Max ADC, RECIST, and the volume of enhanced lesions) and prognosis of GB patients treated by BNCT. Additionally, we treated F98 rat glioma models with BNCT and compared brain sections of the BNCT group with the untreated group using hematoxylin-eosin (H & E) staining.

Methods

Patient population

We performed a retrospective investigation of clinical BNCT to evaluate the effects of therapy and adverse events. From June 2003 to December 2007, we treated a total of 61 GB patients using BNCT. Because 17 of these 61 GB patients (8 females; 9 males) had diffusion MRI at pre- and post-BNCT and had contrast enhancement volumes over 0.7 cm^3 on Gd-MRI, we were able to assess them using fDM. Ten patients were newly diagnosed with GB and 7 patients were recurrent GB cases. The average age was 56.7 years (36–74 years). The average survival time from BNCT was 14.5 months (7.2 - 45.9 months). The average volume of contrast enhancement on Gd-MRIs was 18.8 cm^3 (0.7 - 51.4 cm^3).

Our treatment for GB patients and boron neutron capture therapy protocol

Our treatment for GB patients was surgical resection as much of the tumor as possible, followed by BNCT. Our BNCT protocol was as follows:

Twelve hours before the neutron irradiation, the patients were administered 100 mg/kg or none of sodium borocaptate intravenously for 1 hour. Boronophenylalanine (BPA) of 250 mg/kg was infused continuously to the patients for 1 hours or 700 mg/kg was infused continuously to the patients for 6 hours before the irradiation, and they were positioned for neutron irradiation in the atomic reactor (Kyoto University Research Reactor [KUR] or Japan Atomic Energy Agency Research Reactor 4). Just after termination of continuous BPA infusion for 6 hours, neutrons were irradiated. Between June 2003 and December 2006, no chemotherapy was applied for any of the patients until the tumor progression was confirmed histologically or by

^{18}F-BPA-positron emission tomography [19]. This protocol was approved by the Ethical Committee of Osaka Medical College and also by the Committee for Reactor Medicine in KUR. The indication of BNCT for each candidate was discussed by the latter committee.

MRI examinations

All patients underwent pre-BNCT MRI within 20 days before BNCT and underwent post-BNCT MRI at 2 days after BNCT. MRI examinations were composed of T1-weighted images MRI, T2-weighted images, fluid attenuation inversion recovery (FLAIR) images, Gd-T1-weighted images and diffusion images. MRI was performed on a 1.5-T MRI system (GE; Wisconsin, Milwaukee, USA). MRI sequences included T1-weighted images (TE/TR = 9 ms/2500 ms, slice thickness = 5 mm with 2.5 mm interslice distance, number of excitations [NEX] = 1, matrix size = 256 × 224, and field of view [FOV] = 24 cm), T2-weighted images (TE/TR = 103 ms/2500 ms, slice thickness = 5 mm with 2.5 mm interslice distance, NEX = 1, matrix size = 320 × 192, and FOV = 24 cm), and FLAIR images (inversion time = 2200 ms, TE/TR = 116.7 ms/8800 ms, slice thickness = 5 mm with 2.5 mm interslice distance, NEX = 1, matrix size = 256 × 192, and FOV = 24 cm). In addition, Gd-T1-weighted images (axial: TE/TR = 9 ms/400 ms, slice thickness 5 mm with 2.5 mm interslice distance, NEX = 1, a matrix size of 256 × 224, and FOV = 24 cm) were acquired after contrast injection (Magnevist; Berlex; 0.1 mmol/kg) (Table 1).

Diffusion MRI

Diffusion MRI was collected with TE/TR = 79.3 ms/6400 ms, NEX = 1, slice thickness = 5 mm with 0 mm interslice distance, matrix size = 128 × 192 and a FOV = 24 cm. ADC images were calculated from acquired DWIs with b = 1000 s/mm^2 and b = 0 s/mm^2 images (Table 1). Diffusion images for the three orthogonal directions were combined to calculate an ADC map [20].

Table 1 Summarizing the details of MRI sequences

MRI Sequences	T1	T2	FLAIR	DWI	Gd-T1
TR (ms)	2500	4000	8800	4500	400
TE (ms)	9	103	116.7	67.7	9
inversion time (ms)			2200		
FOV* (cm)	24	24	24	24	24
slice thickness (mm)	5	5	5	5	5
interslice distance (mm)	2.5	2.5	2.5	0	2.5
frequency matrix	256	320	256	128	256
phase matrix	224	192	192	192	224
NEX**	1	1	1	2	1
scan time (s)	107	144	121	64	94

*FOV = field of view **NEX = number of excitations.

fDM analysis

All MRIs were spatially co-registered using the pre-BNCT Gd-MRI as the reference dataset. This step allowed all images of a given patient to be viewed and analyzed from a fixed frame of reference. The co-registration was performed using a "mutual information for automatic multimodality image fusion" (MIAMI FUSE) algorithm [21]. After this co-registration, brain tumors were manually segmented on the Gd-MRIs by a neurosurgeon (R. H.). These segmentations were copied into the contemporary diffusion MRIs and were analyzed using a voxel-by-voxel approach [17,22]. A minimum of 0.7 cm^3 of tumor on Gd-MRI was necessary for eligibility. If a resection cavity was present, it wasn't included within the regions of interest if circumscribed by contrast enhancement. Only voxels present in both the pre-BNCT and post-BNCT tumor volumes were included for fDM analysis. Individual voxels were stratified into three categories based on the change in ADC from the pre-BNCT scan to each time point. Red voxels represent areas within the tumor where ADC increased (> 55 × 10^{-5} mm^2/sec); blue voxels represent decreased ADC (< 55 × 10^{-5} mm^2/sec), and green voxels represent no change (Figure 1). These thresholds represent the 95% confidence intervals for change in ADC for the uninvolved cerebral hemisphere [17]. The percentages of the tumor within these three categories were calculated as V_I, V_D, and V_{NC}, respectively. Other than time-dependent changes of ADC, fDM could automatically assess Min/Max ADC, RECIST, and the volume of enhanced lesions in response to BNCT over time. These analyses were performed using fDM analysis software (*I-Response™-1.0*, Cedara software; Ontario Canada).

Representative case

This patient was newly diagnosed GB with 23.2 months of patients' survival time after BNCT. Depicted images are single slices of Gd-MRI scans at 2 days after BNCT with a pseudocolor overlay of the fDM. Red voxels indicate regions with a significant rise in ADC at 2 days after BNCT compared with pre-BNCT, green regions had no changed ADC, and blue voxels indicate areas of significant decline in ADC (Figure 1A). The scatter plots display data for the entire tumor volume and not just for the depicted slice at 2 days after BNCT, with ADC of the pre-BNCT on the *x*-axis and ADC at 2 days after BNCT on the *y*-axis. The central red line represents unity, and the flanking blue lines represent the 95% confidence interval (CI) (Figure 1B). Other than time-dependent changes of ADC, fDM can automatically assess maximum/minimum ADC, RECIST, and the volume of enhanced lesions on Gd-MRI over time (Figure 1C).

Correlation with all factors assessed by fDM and survival time after BNCT

All factors assessed by fDM are composed of V_I, V_D, V_{NC}, Min/Max ADC, RECIST, and the volume reduction

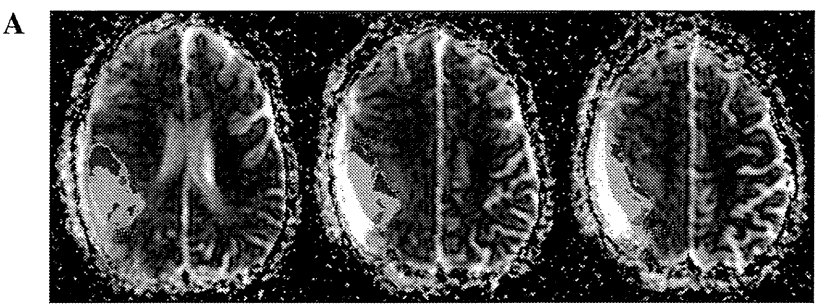

B

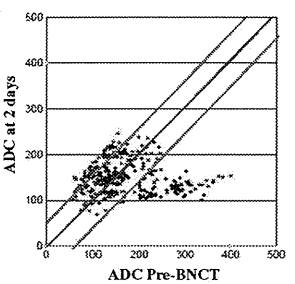

C

All factors assessed by fDM at 2 days after BNCT

V_D (%)	V_I (%)	V_{NC} (%)	$V_D+V_I+V_{NC}$ (%)	Min ADC (10^{-5} mm^2 / sec)	Max ADC (10^{-5} mm^2 / sec)	RECIST (cm)	Volume Reduction Rate (%)
26.8	16.7	56.5	100	55.0	251.0	26.3	29.8

Figure 1 Representative case: Regions of interests were drawn for tumor image by using anatomical images (A). Red voxels represent areas within the tumor where ADC increased (> 55 × 10^{-5} mm^2/sec); blue voxels represent decreased ADC (< 55 × 10^{-5} mm^2/sec), and green voxels represent no change. These thresholds represent the 95% confidence intervals for change in ADC for the uninvolved cerebral hemisphere **(B)**. V_D, V_I, V_{NC}, Min/Max ADC, RECIST, and the volume of enhanced lesions on Gd-MRI over time showed 26.8%, 16.7%, 56.5%, 55.0 10^{-5} mm^2/sec, 251.0 10^{-5} mm^2/sec, 26.3 cm, and 29.8% at 2 days after BNCT, respectively **(C)**.

rate of enhanced lesions. The end point in this study was a survival time after BNCT. Survival analysis utilized log-rank and wilcoxon test. Statistical analysis utilized JMP® Pro 10 (SAS Institute Inc., Cary, NC, USA).

Tumor models

F98 rat glioma cells produce infiltrating tumors in the brains of Fischer rats [23]. The tumors have been shown to be refractory to a number of treatment modalities, including radiation therapy [24]. Based on their *in vivo* histology, the F98 rat glioma cells have been characterized as anaplastic or undifferentiated glioma [25]. In the present study, F98 rat glioma cells were kindly obtained from Prof. Barth (Department of Pathology, the Ohio State University, Columbus, OH, USA). They were routinely cultivated in our laboratory in Dulbecco's Modified Eagle Medium supplemented with 10% fetal bovine serum and penicillin at 37°C in an atmosphere of 5% CO_2. All the materials for the culture medium were purchased from Gibco Invitrogen (Grand Island, NY, USA). Male Fischer rats weighing 200–250 g were anesthetized with an intraperitoneal injection of Nembutal (50 mg/kg) and placed in a stereotactic frame (Model 900, David Kopf Instruments, Tujunga, CA, USA). A midline scalp incision was made and the bregma was identified. A 1mm burr hole was made in the right frontal region of the skull and a 22-gauge needle attached to a 25-μl syringe was inserted into the caudate nucleus using the same stereotactic coordinates, with the needle tip inserted 5 mm into the dura. An injection of 10^3 F98 rat glioma cells in 10 μl of serum free medium was administered at a rate of 1 μl/min. After the infusion, the needle was left in place for 3 min and the burr hole was then covered with bone wax.

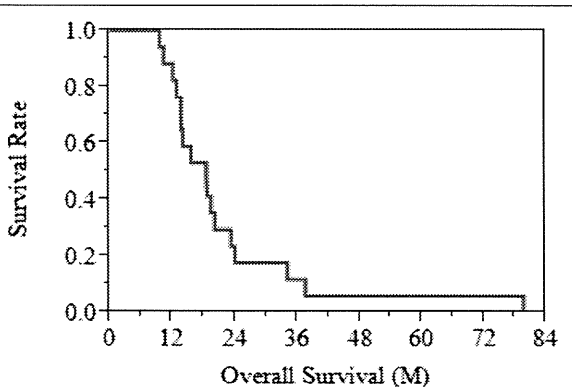

Figure 2 Overall survival of all patients: Median overall survival was 18.5 months (95% CI; 12.9 - 23.2 months).

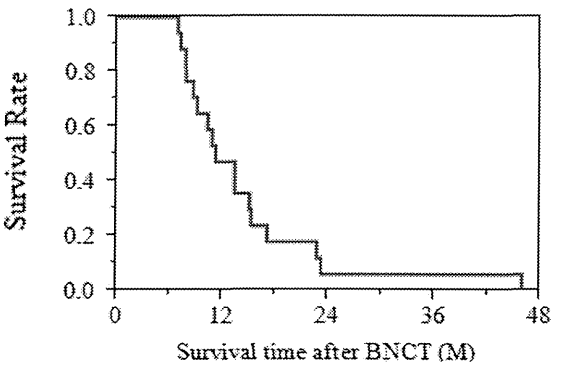

Figure 3 Survival time after BNCT of all patients: Median survival time after BNCT was 11.2 months (95% CI; 7.8 - 15.3 months).

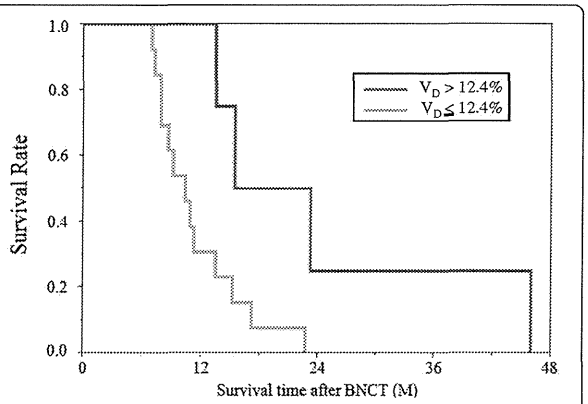

Figure 4 Survival analysis of V_D at 2 days after BNCT: V_D greater than 12.4% at 2 days after BNCT was good response for BNCT (median survival = 19.3 months; 95% CI = 13.4 - 45.9 months) and V_D 12.4% or less at 2 days after BNCT was nonresponse for BNCT (median survival = 10.3 months; 95% CI = 7.8 - 13.4 months).

Histopathological examination

At 2 weeks after implantation, the BNCT group was administered 250 mg/kg body weight of BPA intravenously. An hour and a half after BPA injection, only the BNCT group was irradiated with neutrons at KUR during 1 hour. All rats of both the BNCT group and the untreated group were euthanized by isoflurane 16 days after implantation (i.e., 2 days after BNCT for the BNCT group). The rats were perfused and fixed by 10% formalin; then the brains were dehydrated and embedded in paraffin. The 4-μm sections were stained with hematoxylin and eosin (H & E) for histopathological investigation. We compared sections of the BNCT group with the untreated group using a light microscope (ECLIPSE80i, Nikon, Japan).

Results

MRI examination

In our study, pre-BNCT MRI was performed at 7.9 ± 5.0 (1–20) days before BNCT, and post-BNCT MRI was performed at 2.5 ± 1.6 (1–8) days after BNCT.

Overall survival and survival time after BNCT of all patients

Median overall survival was 18.5 months (95% CI; 12.9 - 23.2 months) (Figure 2) and median survival time after BNCT was 11.2 months (95% CI; 7.8 - 15.3 months) (Figure 3).

Correlation with all factors assessed by fDM and survival time after BNCT

V_D and Min ADC at 2 days after BNCT showed a significant difference using log-rank test and wilcoxon test. However, Min ADC showed over-lap in 95% CI. On the other hand, V_D showed no over-lap in 95% CI (Table 2). V_D greater than 12.4% at 2 days after BNCT was good response for BNCT (median survival = 23.2 months; 95% CI = 13.4 - 45.9 months) and V_D 12.4% or less at 2 days after BNCT was nonresponse for BNCT (median survival = 10.3 months; 95% CI = 7.8 - 13.4 months) (Figure 4). Survival analysis of V_D showed a significant difference (P value = 0.022 by log-rank test and 0.033 by

Table 2 Survival analysis of all factors assessed by fDM

	All factors assessed by fDM													
	V_D (%)		V_I (%)		V_{NC} (%)		Min ADC (10^{-5} mm2/sec)		Max ADC (10^{-5} mm2/sec)		RECIST (cm)		Volume reduction rate of enhanced lesion (%)	
	> 12.4	≤ 12.4	< 3.6	≥ 3.6	< 74.6	≥ 74.6	< 70	≥ 70	< 368	≥ 368	< 40.3	≥ 40.3	< −21.1	≥ −21.1
Median time (M)	19.3	10.3	11.2	12.1	15.3	11	14.3	9.1	11.2	12.1	14.2	10.8	15.1	9.7
95% CI	13.4-	7.8-	7.2-	7.8-	6.9-	7.8-	7.8-	7.2-	7.2-	6.9-	7.8-	7.2-	11.2-	7.2-
(M)	45.9**	13.4**	45.9	15.3	45.9	15.1	22.7**	10.8**	23.2	15.1	45.9	15.1	45.9	15.3
p value log-rank	0.022*		0.521		0.128		0.011*		0.176		0.118		0.143	
wilcoxon	0.033*		0.834		0.35		0.045*		0.413		0.223		0.083	

*V_D and Min ADC at 2 days after BNCT showed a significant difference using log-rank test and wilcoxon test. **However, Min ADC showed over-lap in 95% CI. On the other hand, V_D showed no over-lap in 95% CI.

wilcoxon test). However, V_I, V_{NC}, Max ADC, RECIST, and the volume reduction rate of enhanced lesions at 2 days after BNCT had no correlation with patients' survival time after BNCT (Figure 5, Table 2).

Histopathological examination

Tumor cells in the BNCT group showed swelling of both the nuclei and the cytoplasm compared with the untreated group at 16 days after implantation (i.e., 2 days after BNCT for the BNCT group) (Figure 6).

Discussion

In 1990, Macdonald *et al.* reported criteria for response assessment in glioma [5]. Although these criteria have limitations, they have become widely accepted. However, recent observations have revealed the fundamental limitations of the Macdonald criteria [26,27]. One limitation of the Macdonald criteria is the extended time required to detect change [5,28,29], about 8 to 10 weeks. Another is the discrepancy between contrast enhancement and tumor activity. At the core of Macdonald criteria are changes in contrast enhancement, and all too often, the contrast enhancement of high-grade tumors is perceived as a measure of tumor activity. However, contrast enhancement is nonspecific and primarily reflects a disrupted blood–brain barrier. Contrast enhancement can be influenced by changes in corticosteroid dose and radiologic technique [9,30]. Contrast enhancement can also be induced by a variety of nontumoral processes: inflammation, seizure activity, postsurgical changes, pseudoprogression, radiation necrosis,

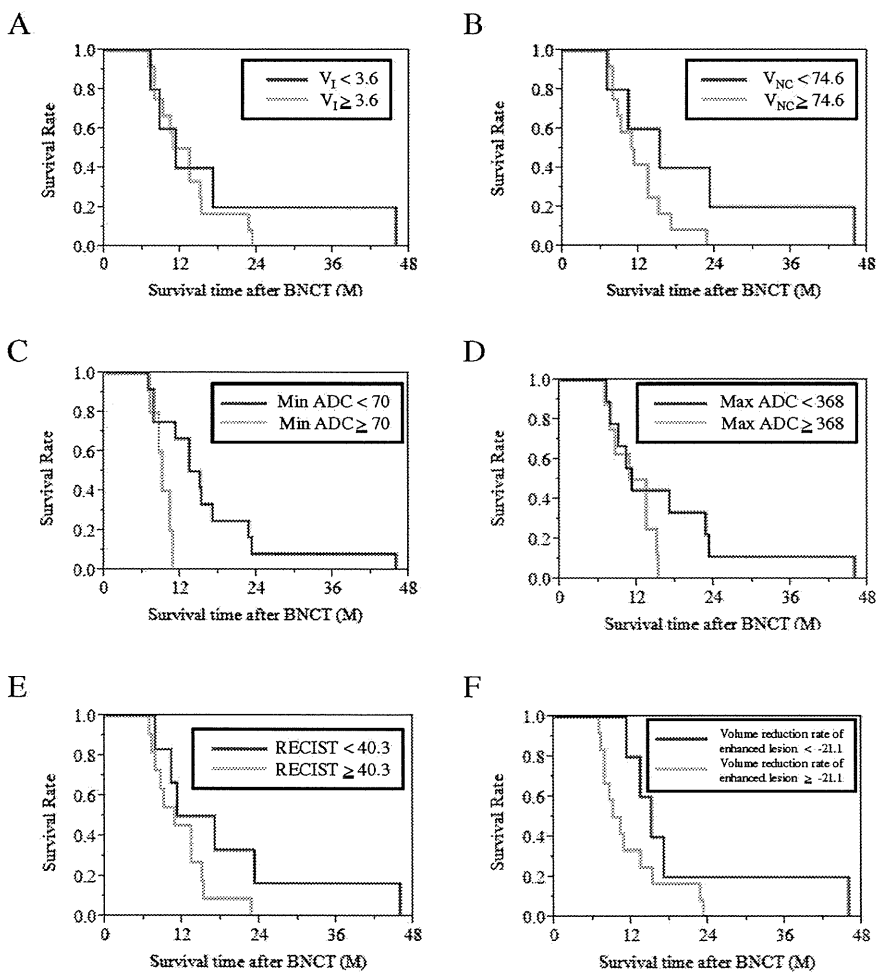

Figure 5 Survival analysis except for V_D at 2 days after BNCT: V_I, V_{NC}, Max ADC, RECIST, and the volume reduction rate of enhanced lesions at 2 days after BNCT (A, B, D, E, and F, respectively) had no correlation with patients' survival time after BNCT using log-rank test and wilcoxon test. Min ADC at 2 days after BNCT **(C)** showed a significant difference using log-rank test and wilcoxon test. However, Min ADC showed over-lap in 95% CI (Table 2).

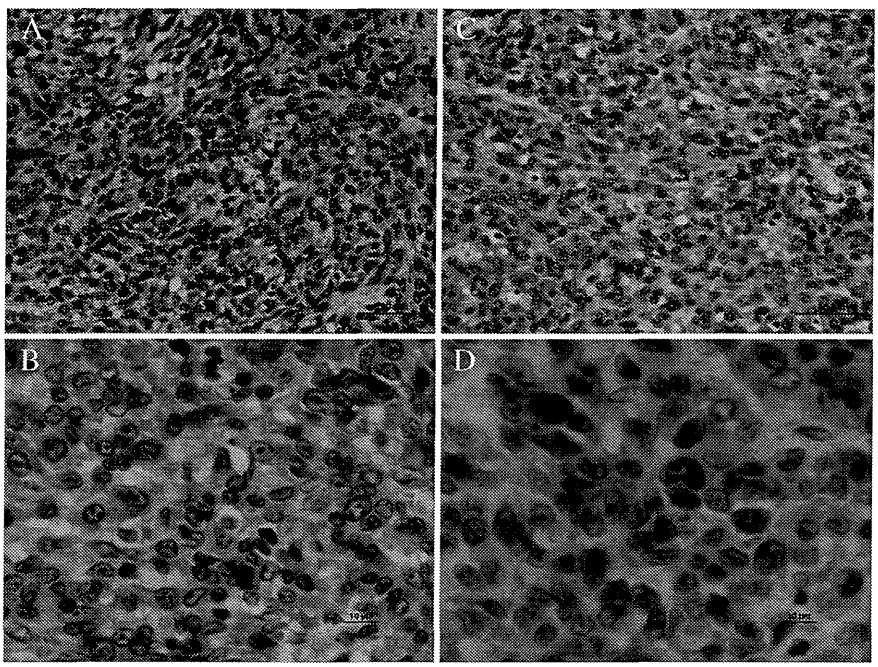

Figure 6 Histopathological examination: Tumor cells in the BNCT group showed the cell swelling of both the nuclei and the cytoplasm (C and D) compared with the untreated group (A and B) at 16 days after the implantation (i.e., at 2 days after BNCT for the BNCT group). (**A** and **C** were at 400-fold. **B** and **D** were 1000-fold magnification).

and pseudoresponse [9,31]. As a result, changes in contrast enhancement cannot be equated with changes in tumor size or tumor growth/activity.

Recently, several novel imaging methods—positron-emission tomography, single-photon emission computerized tomography, MR spectroscopy, and diffusion MRI—have been evaluated for their ability to assess early therapeutic responses independently of late changes in enhanced tumor volume [32,33]. Diffusion MRI detection of cancer treatment response was first successfully reported in a rodent brain tumor model treated with chemotherapy. Additionally, Diffusion MRI has been evaluated in preclinical [11,12,34] and clinical studies [13,34,35]. In 2008, Hamstra *et al.* assessed high-grade glioma with functional diffusion map. They reported that the volume of tumor with increased diffusion by fDM at 3 weeks after the start of radiation therapy was the strongest predictor of patient survival at 1 year [10].

In our study, V_D at 2 days after BNCT was the strongest predictor of GB patients' survival time after BNCT. V_D (= the volume of the voxels with decreased ADC compared with pre-BNCT by fDM) indicates that extracellular free water is relatively decreased for the highest volume of tumor cells. So, this appearance is attributed to tumor progression or tumor cell swelling as previously mentioned in the ***Background***. In our study, day 2 V_D was a good predictor for GB patients treated by BNCT. We attributed this higher V_D to tumor cell swelling rather than tumor progression. In fact, our histopathological study detected tumor cell swelling in the BNCT group compared with the untreated group at 16 days after the implantation (i.e., at 2 days after BNCT for the BNCT group) (Figures 5 and 6). Others have reported tumor cell swelling in the acute stage after BNCT. Kato *et al.* reported the pathological changes of oral squamous cell carcinoma at an early stage after BNCT using nude mouse subcutaneous models. They compared a BNCT group with an untreated group using pathological analysis at 1, 2, and 7 days after BNCT. Compared to the untreated group, oral squamous cell carcinoma in the BNCT group at all early stages showed tumor cell swelling on the H & E stained nude mouse brain sections [36]. Nakagawa *et al.* reported early effects of BNCT on C6 rat glioma models. They compared a BNCT group with an untreated group using pathological analysis at 4days after BNCT. Compared to the untreated group, C6 rat glioma cell in the BNCT group showed cell swelling on the H & E stained rat brain sections [37].

Conclusions

Our study proved that fDM was useful for evaluating the therapeutic efficacy of BNCT in GB patients treated by BNCT. Additionally, fDM could identify response patterns in BNCT-treated GB earlier than a standard radiographic assessment. Early detection of treatment failure can allow a change or supplementation before tumor progression and might lead to an improvement of GB patients' prognosis.

Abbreviations

ADC: Apparent diffusion coefficient; BNCT: Boron neutron capture therapy; BPA: Boronophenylalanine; CI: Confidence interval; fDM: functional diffusion map; FLAIR: Fluid attenuation inversion recovery; FOV: Field of view; GB: Glioblastoma; Gd: Gadolinium; H & E: Hematoxylin and Eosin; KUR: Kyoto university research reactor; Max: Maximum; Min: Minimum; MRI: Magnetic resonance imaging; NEX: Number of excitations; RECIST: Response evaluation criteria in solid tumors; TMZ: Temozolomide.

Competing interests

The authors declare that they have no competing interests.

Authors' contributions

RH carried out all the animal study and the statical analysis, and drafted the manuscript. SK conceived of the study, and participated in its design and coordination and helped to draft the manuscript. MF, S-IM, and TK participated in its design and coordination and helped to draft the manuscript. All authors read and approved the final manuscript.

Acknowledgements

This work was supported by JSPS KAKENHI Grant Number 20791021 to Yoshitaka Yamada, and in part by JSPS KAKENHI Grant Numbers, 23390355 (PI; Shin-ichi Miyatake), 25861294 (PI; Yoko Matsushita) and 23592146 to Shinji Kawabata. We thank to *Cedara Software Corp.* (Ontario Canada) for usage of *I-Response* as a monitor user (agreement #, 2007–02607). And we thank Dr. Barth (Department of Pathology, the Ohio State University) for the provision of F98 rat glioma cells.

Received: 23 May 2013 Accepted: 30 July 2013
Published: 1 August 2013

References

1. Stupp R, Mason WP, van den Bent MJ, Weller M, Fisher B, Taphoorn MJ, Belanger K, Brandes AA, Marosi C, Bogdahn U, *et al*: **Radiotherapy plus concomitant and adjuvant temozolomide for glioblastoma.** *N Engl J Med* 2005, **352**:987–996.
2. Kawabata S, Miyatake S, Nonoguchi N, Hiramatsu R, Iida K, Miyata S, Yokoyama K, Doi A, Kuroda Y, Kuroiwa T, *et al*: **Survival benefit from boron neutron capture therapy for the newly diagnosed glioblastoma patients.** *Appl Radiat Isot* 2009, **67**:S15–18.
3. Miyatake S, Kawabata S, Kajimoto Y, Aoki A, Yokoyama K, Yamada M, Kuroiwa T, Tsuji M, Imahori Y, Kirihata M, *et al*: **Modified boron neutron capture therapy for malignant gliomas performed using epithermal neutron and two boron compounds with different accumulation mechanisms: an efficacy study based on findings on neuroimages.** *J Neurosurg* 2005, **103**:1000–1009.
4. Kawabata S, Miyatake S, Kuroiwa T, Yokoyama K, Doi A, Iida K, Miyata S, Nonoguchi N, Michiue H, Takahashi M, *et al*: **Boron neutron capture therapy for newly diagnosed glioblastoma.** *J Radiat Res* 2009, **50**:51–60.
5. Macdonald DR, Cascino TL, Schold SC Jr, Cairncross JG: **Response criteria for phase II studies of supratentorial malignant glioma.** *J Clin Oncol* 1990, **8**:1277–1280.
6. Wood JR, Green SB, Shapiro WR: **The prognostic importance of tumor size in malignant gliomas: a computed tomographic scan study by the Brain Tumor Cooperative Group.** *J Clin Oncol* 1988, **6**:338–343.
7. Hess KR, Wong ET, Jaeckle KA, Kyritsis AP, Levin VA, Prados MD, Yung WK: **Response and progression in recurrent malignant glioma.** *Neuro Oncol* 1999, **1**:282–288.
8. Taal W, Brandsma D, De Bruin HG, Bromberg JE, Swaak-Kragten AT, Smitt PA, van Es CA, van den Bent MJ: **Incidence of early pseudo-progression in a cohort of malignant glioma patients treated with chemoirradiation with temozolomide.** *Cancer* 2008, **113**:405–410.
9. Brandsma D, van den Bent MJ: **Pseudoprogression and pseudoresponse in the treatment of gliomas.** *Curr Opin Neurol* 2009, **22**:633–638.
10. Hamstra DA, Galban CJ, Meyer CR, Johnson TD, Sundgren PC, Tsien C, Lawrence TS, Junck L, Ross DJ, Rehemtulla A, *et al*: **Functional diffusion map as an early imaging biomarker for high-grade glioma: correlation with conventional radiologic response and overall survival.** *J Clin Oncol* 2008, **26**:3387–3394.
11. Chenevert TL, McKeever PE, Ross BD: **Monitoring early response of experimental brain tumors to therapy using diffusion magnetic resonance imaging.** *Clin Cancer Res* 1997, **3**:1457–1466.
12. Poptani H, Puumalainen AM, Grohn OH, Loimas S, Kainulainen R, Yla-Herttuala S, Kauppinen RA: **Monitoring thymidine kinase and ganciclovir-induced changes in rat malignant glioma in vivo by nuclear magnetic resonance imaging.** *Cancer Gene Ther* 1998, **5**:101–109.
13. Mardor Y, Roth Y, Lidar Z, Jonas T, Pfeffer R, Maier SE, Faibel M, Nass D, Hadani M, Orenstein A, *et al*: **Monitoring response to convection-enhanced taxol delivery in brain tumor patients using diffusion-weighted magnetic resonance imaging.** *Cancer Res* 2001, **61**:4971–4973.
14. Ellingson BM, Cloughesy TF, Lai A, Nghiemphu PL, Liau LM, Pope WB: **Quantitative probabilistic functional diffusion mapping in newly diagnosed glioblastoma treated with radiochemotherapy.** *Neuro Oncol* 2013, **15**:382–390.
15. Ellingson BM, Cloughesy TF, Zaw T, Lai A, Nghiemphu PL, Harris R, Lalezari S, Wagle N, Naeini KM, Carrillo J, *et al*: **Functional diffusion maps (fDMs) evaluated before and after radiochemotherapy predict progression-free and overall survival in newly diagnosed glioblastoma.** *Neuro Oncol* 2012, **14**:333–343.
16. Armitage PA, Schwindack C, Bastin ME, Whittle IR: **Quantitative assessment of intracranial tumor response to dexamethasone using diffusion, perfusion and permeability magnetic resonance imaging.** *Magn Reson Imaging* 2007, **25**:303–310.
17. Hamstra DA, Chenevert TL, Moffat BA, Johnson TD, Meyer CR, Mukherji SK, Quint DJ, Gebarski SS, Fan X, Tsien CI, *et al*: **Evaluation of the functional diffusion map as an early biomarker of time-to-progression and overall survival in high-grade glioma.** *Proc Natl Acad Sci U S A* 2005, **102**:16759–16764.
18. Lyng H, Haraldseth O, Rofstad EK: **Measurement of cell density and necrotic fraction in human melanoma xenografts by diffusion weighted magnetic resonance imaging.** *Magn Reson Med* 2000, **43**:828–836.
19. Miyashita M, Miyatake S, Imahori Y, Yokoyama K, Kawabata S, Kajimoto Y, Shibata MA, Otsuki Y, Kirihata M, Ono K, Kuroiwa T: **Evaluation of fluoride-labeled boronophenylalanine-PET imaging for the study of radiation effects in patients with glioblastomas.** *J Neurooncol* 2008, **89**:239–246.
20. Le Bihan D, Breton E, Lallemand D, Aubin ML, Vignaud J, Laval-Jeantet M: **Separation of diffusion and perfusion in intravoxel incoherent motion MR imaging.** *Radiology* 1988, **168**:497–505.
21. Meyer CR, Boes JL, Kim B, Bland PH, Zasadny KR, Kison PV, Koral K, Frey KA, Wahl RL: **Demonstration of accuracy and clinical versatility of mutual information for automatic multimodality image fusion using affine and thin-plate spline warped geometric deformations.** *Med Image Anal* 1997, **1**:195–206.
22. Moffat BA, Chenevert TL, Meyer CR, McKeever PE, Hall DE, Hoff BA, Johnson TD, Rehemtulla A, Ross BD: **The functional diffusion map: an imaging biomarker for the early prediction of cancer treatment outcome.** *Neoplasia* 2006, **8**:259–267.
23. Barth RF: **Rat brain tumor models in experimental neuro-oncology: the 9L, C6, T9, F98, RG2 (D74), RT-2 and CNS-1 gliomas.** *J Neurooncol* 1998, **36**:91–102.
24. Biston MC, Joubert A, Adam JF, Elleaume H, Bohic S, Charvet AM, Esteve F, Foray N, Balosso J: **Cure of Fisher rats bearing radioresistant F98 glioma treated with cis-platinum and irradiated with monochromatic synchrotron X-rays.** *Cancer Res* 2004, **64**:2317–2323.
25. Kobayashi N, Allen N, Clendenon NR, Ko LW: **An improved rat brain-tumor model.** *J Neurosurg* 1980, **53**:808–815.
26. Henson JW, Ulmer S, Harris GJ: **Brain tumor imaging in clinical trials.** *AJNR Am J Neuroradiol* 2008, **29**:419–424.
27. Sorensen AG, Batchelor TT, Wen PY, Zhang WT, Jain RK: **Response criteria for glioma.** *Nat Clin Pract Oncol* 2008, **5**:634–644.
28. Miller AB, Hoogstraten B, Staquet M, Winkler A: **Reporting results of cancer treatment.** *Cancer* 1981, **47**:207–214.
29. Therasse P, Arbuck SG, Eisenhauer EA, Wanders J, Kaplan RS, Rubinstein L, Verweij J, Van Glabbeke M, van Oosterom AT, Christian MC, Gwyther SG: **New guidelines to evaluate the response to treatment in solid tumors. European Organization for Research and Treatment of Cancer, National Cancer Institute of the United States, National Cancer Institute of Canada.** *J Natl Cancer Inst* 2000, **92**:205–216.
30. Watling CJ, Lee DH, Macdonald DR, Cairncross JG: **Corticosteroid-induced magnetic resonance imaging changes in patients with recurrent malignant glioma.** *J Clin Oncol* 1994, **12**:1886–1889.

31. Kumar AJ, Leeds NE, Fuller GN, Van Tassel P, Maor MH, Sawaya RE, Levin VA: **Malignant gliomas: MR imaging spectrum of radiation therapy- and chemotherapy-induced necrosis of the brain after treatment.** *Radiology* 2000, **217**:377–384.
32. Spence AM, Mankoff DA, Muzi M: **Positron emission tomography imaging of brain tumors.** *Neuroimaging Clin N Am* 2003, **13**:717–739.
33. Van de Wiele C, Lahorte C, Oyen W, Boerman O, Goethals I, Slegers G, Dierckx RA: **Nuclear medicine imaging to predict response to radiotherapy: a review.** *Int J Radiat Oncol Biol Phys* 2003, **55**:5–15.
34. Chenevert TL, Stegman LD, Taylor JM, Robertson PL, Greenberg HS, Rehemtulla A, Ross BD: **Diffusion magnetic resonance imaging: an early surrogate marker of therapeutic efficacy in brain tumors.** *J Natl Cancer Inst* 2000, **92**:2029–2036.
35. Mardor Y, Pfeffer R, Spiegelmann R, Roth Y, Maier SE, Nissim O, Berger R, Glicksman A, Baram J, Orenstein A, *et al*: **Early detection of response to radiation therapy in patients with brain malignancies using conventional and high b-value diffusion-weighted magnetic resonance imaging.** *J Clin Oncol* 2003, **21**:1094–1100.
36. Kamida A, Obayashi S, Kato I, Ono K, Suzuki M, Nagata K, Sakurai Y, Yura Y: **Effects of boron neutron capture therapy on human oral squamous cell carcinoma in a nude mouse model.** *Int J Radiat Biol* 2006, **82**:21–29.
37. Nakagawa N, Akai F, Fukawa N, Fujita Y, Suzuki M, Ono K, Taneda M: **Early effects of boron neutron capture therapy on rat glioma models.** *Brain Tumor Pathol* 2007, **24**:7–13.

doi:10.1186/1748-717X-8-192
Cite this article as: Hiramatsu *et al.*: Identification of early and distinct glioblastoma response patterns treated by boron neutron capture therapy not predicted by standard radiographic assessment using functional diffusion map. *Radiation Oncology* 2013 8:192.

Submit your next manuscript to BioMed Central and take full advantage of:

- Convenient online submission
- Thorough peer review
- No space constraints or color figure charges
- Immediate publication on acceptance
- Inclusion in PubMed, CAS, Scopus and Google Scholar
- Research which is freely available for redistribution

Submit your manuscript at
www.biomedcentral.com/submit

BioMed Central

Miyata et al. Radiation Oncology 2014, 9:51
http://www.ro-journal.com/content/9/1/51

RADIATION ONCOLOGY

RESEARCH Open Access

The roles of platelet-derived growth factors and their receptors in brain radiation necrosis

Tomo Miyata[1], Taichiro Toho[1], Naosuke Nonoguchi[1], Motomasa Furuse[1], Hiroko Kuwabara[2], Erina Yoritsune[1], Shinji Kawabata[1], Toshihiko Kuroiwa[1] and Shin-Ichi Miyatake[1*]

Abstract

Background: Brain radiation necrosis (RN) occurring after radiotherapy is a serious complication. We and others have performed several treatments for RN, using anticoagulants, corticosteroids, surgical resection and bevacizumab. However, the mechanisms underlying RN have not yet been completely elucidated. For more than a decade, platelet-derived growth factors (PDGFs) and their receptors (PDGFRs) have been extensively studied in many biological processes. These proteins influence a wide range of biological responses and participate in many normal and pathological conditions. In this study, we demonstrated that PDGF isoforms (PDGF-A, B, C, and D) and PDGFRs (PDGFR-α and β) are involved in the pathogenesis of human brain RN. We speculated on their roles, with a focus on their potential involvement in angiogenesis and inflammation in RN.

Methods: Seven surgical specimens of RN, obtained from 2006 to 2013 at our department, were subjected to histopathological analyses and stained with hematoxylin and eosin. We qualitatively analyzed the protein expression of each isoform of PDGF by immunohistochemistry. We also examined their expression with double immunofluorescence.

Results: All PDGFs were expressed in macrophages, microglia, and endothelial cells in the boundary of the core of RN, namely, the perinecrotic area (PN), as well as in undamaged brain tissue (UB). PDGF-C, D and PDGFR-α were also expressed in reactive astrocytes in PN. PDGFs and PDGFR-α were scarcely detected in UB, but PDGFR-β was specifically expressed in endothelial cells not only in PN but also in UB.

Conclusions: PDGFs/PDGFRs play critical roles in angiogenesis and possibly in inflammation, and they contribute to the pathogenesis of RN, irrespective of the original tumor pathology and applied radiation modality. Treatments for the inhibition of PDGF-C, PDGF-D, and PDGFR-α may provide new approaches for the treatment of RN induced by common radiation therapies.

Keywords: Angiogenesis, Brain radiation necrosis, Inflammation, Platelet-derived growth factors, Platelet-derived growth factor receptors

Background

Higher radiation doses to tumors result in good local tumor control and improvement in overall survival. On the other hand, radiation necrosis (RN) in the brain occurring after radiotherapy for brain tumors as well as for head and neck cancers is a serious complication that decreases the quality of life in patients. The mechanisms underlying RN have not been completely elucidated. In a previous study we showed that RN specimens stained with hematoxylin and eosin (H&E) typically show marked angiogenesis, so-called telangiectasis, microbleeding, and interstitial edema, probably caused by leakage of plasma from leaky angiogenesis into the surrounding necrotic core—namely, the perinecrotic area (PN) [1].

We and others have applied several treatments for RN, such as anticoagulants, vitamin E, corticosteroids, and surgical resection [2-4]. The typical MRI of symptomatic RN from case 3 demonstrated rapid shrinkage of the perilesional edema after surgical treatment [see Additional file 1 and Table 1]. After surgical resection for the only

* Correspondence: neu070@poh.osaka-med.ac.jp
[1]Department of Neurosurgery, Osaka Medical College, 2-7 Daigaku-machi, Takatsuki City, Osaka 569-8686, Japan
Full list of author information is available at the end of the article

BioMed Central

© 2014 Miyata et al.; licensee BioMed Central Ltd. This is an Open Access article distributed under the terms of the Creative Commons Attribution License (http://creativecommons.org/licenses/by/2.0), which permits unrestricted use, distribution, and reproduction in any medium, provided the original work is properly credited. The Creative Commons Public Domain Dedication waiver (http://creativecommons.org/publicdomain/zero/1.0/) applies to the data made available in this article, unless otherwise stated.

Table 1 Clinical features of patients with symptomatic radiation necrosis

Pt.	Age (y)	Sex	Original dis.	Radiation[a]	Resection area (lobe)	Duration[b]	Chemo
1	46	F	SCC.	XRT (60 Gy), BNCT (13.9 Gy-Eq)	Temporal	7	MTX
2	78	M	Sal. Duc. Ca.	XRT (60 Gy), BNCT (13.9 Gy-Eq)	Frontotemporal	20	-
3	18	M	GBM	XRT (IMRT) (74 Gy)	Parietal	37	-
4	63	F	GBM	XRT (24 Gy), BNCT (13 Gy-Eq)	Frontoparietal	4	-
5	34	M	GBM	XRT (24 Gy), BNCT (13 Gy-Eq)	Frontal	6	-
6	56	F	GBM	Proton + XRT (total 90 Gy)	Temporoparietal	10	ACNU
7	46	F	Ade. Ca.	XRT (30 Gy), SRS (55 Gy, 65 Gy)	Frontal	32	Herceptin

Pt, patient; *y*, year; *F*, female; *M*, male; *Original dis*, original disease; *SCC*, Squamous cell carcinoma; *Sal. Duc. Ca*, salivary ductal carcinoma; *GBM*, glioblastoma; *Ade. Ca*, adenocarcinoma; *XRT*, X-ray radiation treatment; *IMRT* ,intensity modulated radiation therapy; *BNCT*, boron neutron capture therapy; *Proton*, proton beam therapy; *MTX*, methotrexate; *ACNU*, nimustin; *Herceptin*, trastuzumab;
[a]In Pt. 1 and 2, the temporal lobe was included in the irradiation field and in Pt. 3, 4, 5, and 6, local radiation therapy was administered. Pt. 7 had received whole brain irradiation and received SRS twice. In BNCT, the presented dose is the peak point dose for the normal brain.
[b]Months between termination of the last radiotherapy and onset of symptoms caused by radiation necrosis.

enhanced lesion, the perilesional edema decreased rapidly compared with preoperative MRI. This rapid shrinkage of the perilesional edema after surgical treatment was also observed in other cases. In addition, bevacizumab, an antibody for vascular endothelial growth factor (VEGF), has recently shown promising effects on symptomatic brain RN and symptomatic pseudo-progression [5,6]. However, in some cases, treatment with bevacizumab was not sufficient to resolve RN. Some RN cases recurred as RN even after temporary remission by bevacizumab treatment [7].

Recent experiments have shown that demyelination and damage of the normal vasculatures and the appearance of abnormal vasculatures around necrotic foci are major issues in the development of RN [8,9]. In addition, we previously reported that hypoxia-inducible factor 1α (HIF-1α) and VEGF are key molecules in RN [1]. In a later study, we tried to determine whether not only HIF-1α and VEGF, but also proinflammatory cytokines such as IL-1α, IL-6, TNF-α, and NFκB, might play significant roles in RN, since these cytokines were produced by CD68- and hGLUT5-positive microglia and/or macrophages accumulated in PN (in submission).

The platelet-derived growth factors (PDGFs) signaling pathway, which has been extensively studied and shown to play critical roles in many biological processes, is mediated through tyrosine kinase receptors (PDGFR-α, PDGFR-β) [10,11]. There are five members of the PDGF family: PDGF-A, B, and AB, and the recently discovered PDGF-C and D. So far, no heterodimers involving the PDGF-C and D chains have been described. PDGF-A binds only PDGFR-α, whereas PDGF-B activates PDGFR-α, αβ, and β. PDGF-A, B, and C activate PDGFR-α and αβ, while PDGF-D specifically binds to and activates its cognate receptor PDGFR-β. In other words, according to published data, PDGFR-α binds PDGF-A, B, AB, and C, whereas PDGFR-β binds PDGF-B and D [10,12,13].

In addition, PDGF-A and B are secreted in their active forms, while PDGF-C and D are secreted as inactive forms requiring activation for their function [14]. Interestingly, several reports have shown that the structure and biological function of PDGFs are quite similar to those of VEGF [15]. Therefore, the PDGF family is sometimes referred to as the VEGF family. Nevertheless, in recent years it was revealed that the angiogenic pathway induced by PDGF-C is, in large part, VEGF-independent [16].

Based on these findings, in this retrospective study we performed histopathological and immunohistochemical analyses on 7 human RN specimens from patients who we had treated surgically from 2006 to 2013 at our department. We here describe the findings common to all 7 of these specimens, and demonstrate which type of cells produce PDGFs and which type express the PDGFRs. We also evaluated the roles of PDGFs/PDGFRs in brain RN.

Methods

Case selection

Seven surgical specimens, obtained from 2006 to 2013, were submitted for histopathological analysis, staining with H&E, and immunohistochemistry. All the patients had received radiotherapy, including X-ray treatment (XRT), stereotactic radiosurgery (SRS), proton beam therapy, and boron neutron capture therapy (BNCT). The primary diseases were 4 glioblastomas, 2 head and neck cancers, and 1 metastatic brain tumor derived from breast cancer.

In this study we selected the area as radiation necrosis with extensive necrotic area with the boundary of extensive angiogenesis and edema, which is continuous to undamaged brain tissue, as mentioned in Background.

For the 2 patients with head and neck cancers, radiotherapy was used to treat the parotid lesions and the temporal lobe was included in the irradiation field. Therefore, there were no tumor cells in the brain, indicating pure brain RN. The patient characteristics are detailed in Table 1.

Histological and immunohistochemical staining

Histological and immunohistochemical analyses were performed on paraffin sections in which we observed the presence of RN by H&E staining. Each section was immunostained with the following antibodies: PDGF-A (1:20; R&D Systems, USA), PDGF-B (1:20; Abcam, Japan), PDGF-C (1:100; R&D Systems), PDGF-D (1:50; R&D Systems), PDGFR-α (1:20; R&D Systems), and PDGFR-β (1:50; R&D Systems) (Table 2). We routinely use a pressure cooker for 4 minutes to retrieve all the antigens. Endogenous peroxidase was blocked with 0.03% hydrogen peroxide for 40 minutes at room temperature. We used the ABC technique (Vector Laboratories, USA) for all of these antigens, before DAB (3, 3′ diaminobenzidine tetrahydrochloride (Wako Pure Chemical Industries, Japan)). The sections were counterstained with hematoxylin 3G (Sakura Finetek, Japan) and mounted.

Immunofluorescence

Double immunofluorescence was performed using the following antibody combinations: PDGF-C and GFAP (1:25; Dako, Denmark), CD68 (1:25; Epitomics, USA), hGLUT5 (1:50; IBL, Japan), or CD45 (1:50; Epitomics); PDGF-D and GFAP, CD68, hFLUT5, or CD45; PDGFR-α and GFAP, CD68, hGLUT5, or CD31 (1:20; Dako, Denmark); and PDGFR-β and GFAP, CD68, hGLUT5, or CD31.

GFAP, CD68, hGLUT5, CD45, and CD31 were adopted as markers for astrocytes, monocytes, microglia, lymphocytes, and endothelial cells, respectively. All sections were incubated with their respective antibodies for 24 hours with CD68, hGLUT5, and GFAP, and for 48 hours with PDGF-A, B, C, D, and PDGFR-α and β. Then, after washing the primary antibodies, Alexa Fluor 488 (1:25; Molecular Probes, USA) or Alexa Fluor 546 (1:25; Molecular Probes) was used (Table 3). Finally, the sections were examined using an LSM510 laser scanning confocal microscope (Carl Zeiss, Germany).

Table 2 List of primary antibodies used

Antibody	Clone	Sources	Type	Dilution
PDGF-A		R&D Systems, Minneapolis, MN	p/g	1:20
PDGF-B	MM0014-5 F66	Abcam Cambridge, MA	m/m	1:20
PDGF-C		R&D Systems, Minneapolis, MN	p/g	1:100
PDGF-D		R&D Systems, Minneapolis, MN	p/g	1:50
PDGFR-α		R&D Systems, Minneapolis, MN	p/g	1:20
PDGFR-β		R&D Systems, Minneapolis, MN	p/g	1:50
CD68	KP-1	Dako, Glostrup, Denmark	m/m	1:25
hGLUT5		IBL, Tokyo, Japan	p/r	1:50
GFAP	6 F2	Dako, Glostrup, Denmark	m/m	1:25
CD45	EP322Y	Eptomics, Burlingame, CA	m/r	1:50
CD31	JC70A	Dako, Glostrup, Denmark	m/m	1:20

p/g polyclonal goat; *p/r*, polyclonal rabbit; *m/r*, monoclonal rabbit; *m/m*, monoclonal mouse.

Statistical analysis

We assessed the frequency of expression of PDGFs semi-quantitatively by the following method. Five fields of each PDGF isoform in which abnormal angiogenesis was detected were randomly selected with a microscope. PDGF-positive mononuclear cells were counted. We observed 7 cases and, to reduce bias, used two observers to count the cells. One observer, who was blinded to the patients' clinical and pathological information, evaluated the results of immunohistochemical staining. The ratios of PDGF-positive cells per total cells in each field were calculated, and we statistically analyzed the data with Steel-Dwass tests using JMP Pro 10 (SAS Institute, USA). The results revealed that PDGF-C and D showed higher frequency of expression than PDGF-A and B in PN. The difference was statistically significant.

Ethical approval

This study was approved by an institutional committee of Osaka Medical College. The research was in compliance with the Helsinki Declaration.

Results

Expression of PDGFs

Figure 1 shows the results of H&E staining and immunohistochemistry from case 1. H&E staining revealed a necrotic

Table 3 Double immunofluorescence combinations

Primary	Dilution	Secondary	Primary	Dilution	Secondary
PDGF-C	1:50	F488	CD68	1:25	F546
PDGF-C	1:50	F488	hGLUT5	1:50	F546
PDGF-C	1:50	F488	GFAP	1:25	F546
PDGF-C	1:50	F488	CD45	1:50	F546
PDGF-D	1:20	F488	CD68	1:25	F546
PDGF-D	1:20	F488	hGLUT5	1:50	F546
PDGF-D	1:20	F488	GFAP	1:25	F546
PDGF-D	1:20	F488	CD45	1:50	F546
PDGFR-α	1:10	F488	CD68	1:25	F546
PDGFR-α	1:10	F488	hGLUT5	1:50	F546
PDGFR-α	1:10	F488	GFAP	1:25	F546
PDGFR-α	1:10	F488	CD31	1:20	F546
PDGFR-β	1:20	F488	CD68	1:25	F546
PDGFR-β	1:20	F488	hGLUT5	1:50	F546
PDGFR-β	1:20	F488	GFAP	1:25	F546
PDGFR-β	1:20	F488	CD31	1:20	F546

Primary, primary antibody; *Secondary*, secondary antibody; *F488*, Alexa Fluor 488; *F546*, Alexa Fluor 546.

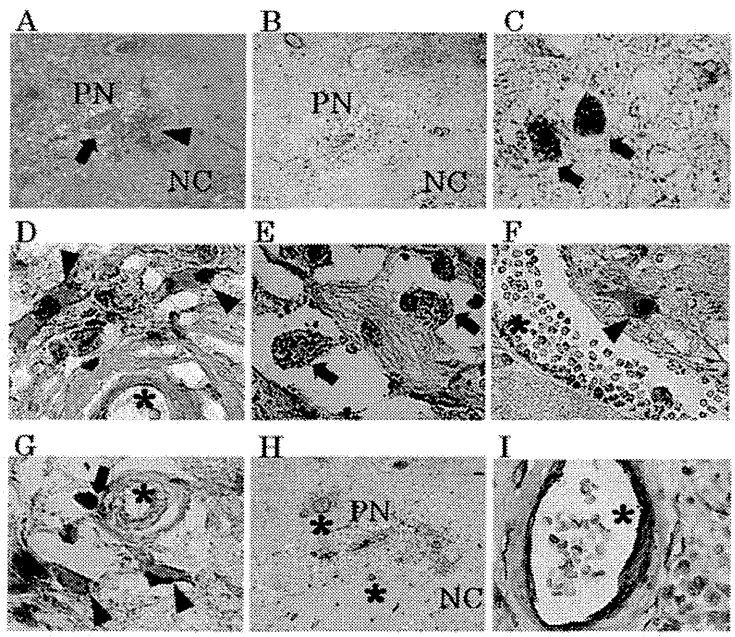

Figure 1 Results of hematoxylin and eosin staining (H&E) and immunohistochemistry from case 1. H&E staining **(A)** revealed a necrotic core (NC) and perinecrotic area (PN), including micro bleeding (**A**, arrowhead) and abnormal angiogenesis (**A**, arrow). Immunostaining results for PDGF-C are presented as a representative example **(B)**. PDGF-C **(C and D)**, D **(E and F)** and PDGFR-α **(G)** were produced by monocytic cells (**C**, **E**, **G**, arrow) and reactive astrocytic cells (**D**, **F**, **G**, arrowhead) in PN. On the other hand, PDGFR-β **(H and I)** was expressed mainly in endothelial cells **(H and I*)**. There was partially nonspecific staining in NC **(B)** or around blood vessels **(I)**. Original magnification, **A**, **B** and **H** × 40, **C**, **D**, **E**, **F**, **G** and **I** × 200.

core (NC) (Figure 1A. NC) and PN (Figure 1A. PN), in which micro bleeding (Figure 1A. arrowhead) and abnormal angiogenesis (Figure 1A. arrow) were confirmed. PDGF-A, B, C, and D-positive cells were detected in PN. The results of immunostaining for PDGF-C are shown as a typical example of these distribution analyses (Figure 1B, C, D). Morphologically, PDGF-A and B were produced by some monocytic cells [see Additional file 2] in PN. On the other hand, PDGF-C and D (Figure 1E, F) were produced by many monocytic cells (arrows in Figure 1C, E), reactive astrocytic cells (arrowheads in Figure 1D, F), and endothelial cells (Figure 1D*). PDGF-A, B, C, and D were scarcely detectable in UB (Figure 2).

These relationships among the expression of PDGFs are summarized in Table 4. These relationships were also confirmed with other specimens [see Additional file 3].

Our statistical analysis revealed that PDGF-C and D showed higher frequencies of expression than PDGF-A and B in PN. The difference was statistically significant ($p < 0.0001$, Steel-Dwass test) (Figure 3). We also grouped the cases into a GBM group (cases 3, 4, 5, 6) and non-GBM group (cases 1, 2, 7) and analyzed the differences in protein expression between them. No statistically significant differences in the expression of any of the isoforms were observed between the two groups by the Steel-Dwass test [see Additional file 4]. Therefore, we considered that these primary diseases did not affect the expression of PDGFs.

Double immunofluorescence from case 1 revealed that PDGF-C or D-positive cells were merged with many cells positive for CD68 (Figure 4A, E), GFAP (Figure 4B, F), hGLUT5 (Figure 4C, G), and CD45 (Figure 4D, H).

H&E staining, immunohistochemistry, and double immunofluorescence also showed similar tendencies in other specimens with symptomatic RN [see Additional files 3, and 5].

Expression of PDGFRs

PDGFR-α was expressed in endothelial cells (Figure 1G*), monocytic cells (Figure 1G arrow), and reactive astrocytic cells (Figure 1G, arrowhead) in PN. PDGFR-β was expressed mainly in endothelial cells (Figure 1H, I*). PDGFR-α was not expressed in any types of cells in UB (Figure 2E), but PDGFR-β was detected in endothelial cells in both PN and UB (Figure 2F).

Double immunofluorescence revealed that PDGFR-α and β were strongly expressed in CD31-positive cells (Figure 5D, I). PDGFR-β-positive cells were merged specifically with endothelial cells (Figure 5E, G, H, I and J, *), but PDGFR-α-positive cells were merged with cells positive for CD68 (Figure 5A), GFAP (Figure 5B), hGLUT5 (Figure 5C), and CD45 (Figure 5E) in PN.

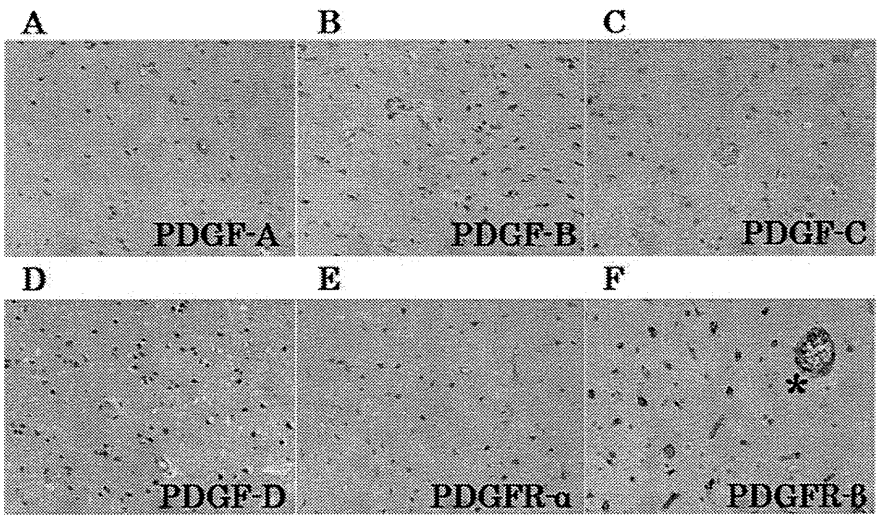

Figure 2 Representative results of immunostaining of undamaged brain tissue (UB). PDGF-A, B, C, D and PDGFR-α were scarcely detectable in UB **(A through E)**. PDGFR-β **(F)** was specifically expressed in endothelial cells in UB. Many normal cerebral blood vessels stained with PDGFR-β **(F *)** were detected in UB. Original magnification, ×200.

These findings from case 1 were confirmed in other specimens with symptomatic RN [see Additional file 6].

Double immunofluorescence revealed partially non-specific staining, especially in endothelial cells (Figures 4, and 5*). In cases where immunofluorescence was performed with GFAP alone, vascular endothelial cells were not stained [see Additional file 7]. These findings were also observed in other specimens.

Discussion

PDGFs are a group of multifunctional proteins with a wide variety of effects. They have important physiologic functions in embryonic and organ development, have been implicated in a wide variety of pathological processes, including proliferation, differentiation, and fibrogenesis, and are essential for the stability of normal blood vessel formation [16-19]. However, the overexpression of

Table 4 Expression of PDGFs/PDGFRs in two areas of the brain

	UB			PN		
	Mono	Astro	Endo	Mono	Astro	Endo
PDGF-A	-	-	-	+	-	+
PDGF-B	-	-	-	+	-	+
PDGF-C	-	-	-	+	+	+
PDGF-D	-	-	-	+	+	+
PDGFR-α	-	-	-	+	+	+
PDGFR-β	-	-	+	-	-	+

UB, undamaged brain area; *PN*, perinecrotic area; *Mono*, monocytes, including macrophages, microglia and lymphocytes *Astro*, reactive astrocytes; *Endo*, endothelial cells ; -, not expressed; +, expressed.

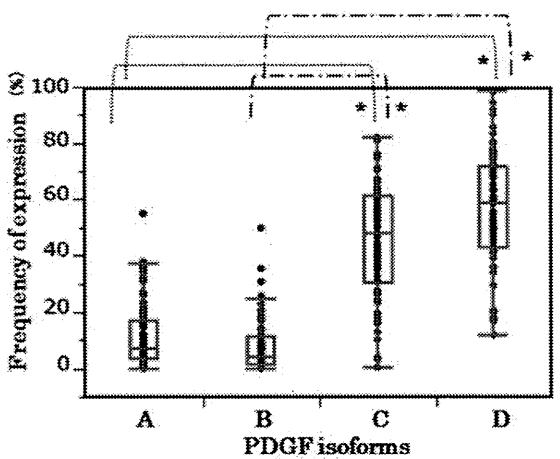

Figure 3 Frequency of expression. We assessed the frequency of expression of PDGFs semi-quantitatively by the following method. Five fields of each PDGF isoform, in which abnormal angiogenesis were detected, were randomly selected with a microscope. The PDGF-positive mononuclear cells were counted. We observed all 7 cases and performed the counting using two observers to reduce bias. One observer, who was blind to the patients' clinical and pathological information, evaluated the results of the immunohistochemical staining. The ratios of PDGF-positive cells to total cells in each field were calculated and were statistically analyzed using Steel-Dwass tests with JMP Pro 10 (SAS Institute Inc, Cary, NC, USA). Statistical analysis revealed that PDGF-C and D showed higher frequency of expression in the PN specimens than did PDGF-A and B. The difference was statistically significant (*$p < 0.0001$, Steel-Dwass test).

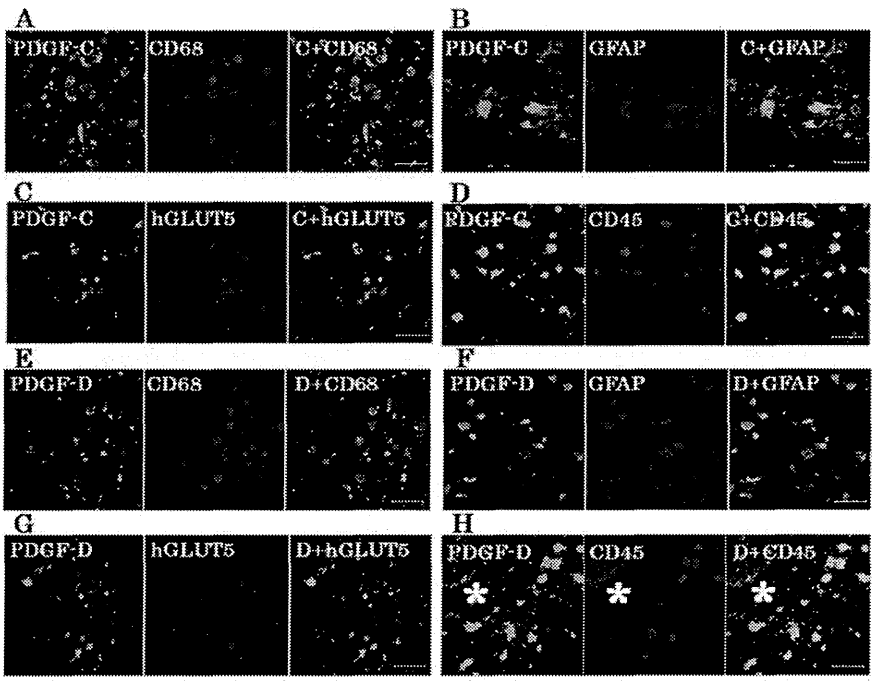

Figure 4 Double immunofluorescence staining. The results of double immunofluorescence staining from case 1 revealed that PDGF-C or D-positive cells were merged with many CD68 **(A, E)**, GFAP **(B, F)**, hGLUT5 **(C, G)**, and CD45 **(D, H)** -positive cells in PN. Some PDGF-C or D-positive cells did not express CD68, GFAP, hGLUT5 or CD45 and vice versa. Endothelial cells **(*)** were nonspecifically stained with secondary fluorescence antibody. The scale bar represents 50 μm.

PDGFs has adverse effects. Previous studies also have demonstrated that various cell types, including macrophages, fibroblasts, pericytes, and capillary endothelial cells, express PDGFs [20,21]. Deuel et al. also reported that a macrophage-derived PDGF induces chemotaxis and the proliferation of monocytes and fibroblasts during inflammation and wound repair [22].

This is the first study to explore the expression of PDGF isoforms and PDGFRs in human brain RN. Our results have shown that all PDGFs and PDGFRs were expressed in brain RN, and that PDGFs and PDGFRα were primarily expressed by macrophages, microglia, reactive astrocytes, lymphocytes, and endothelial cells in PN. These findings suggest that the activation of PDGFs is coincident with inflammation, angiogenesis, and fibrogenesis in the pathophysiology of RN.

Our recent study revealed that CD45-positive lymphocytes expressing CXCR4 might be drawn into PN from peripheral blood by chemotaxis, but they do not express proinflammatory cytokines, and their roles in RN remain unclear (submitted for publication). However, in the present study, CD45-positive lymphocytes produced PDGF-C and -D. These results suggest that CD45-positive lymphocytes in PN do not produce proinflammatory cytokines but may play significant indirect roles in angiogenesis and/or inflammation.

The highest differences of expression among PDGFs on brain RN were observed in PDGF-C and D (Figure 3 and Additional file 4). In this study, the expressions of PDGF-C and D were significantly higher than the expressions of PDGF-A and B in PN. Our current immunohistochemical study has further revealed that inflammatory cells, including macrophages, microglia, and even lymphocytes, were gathered in PN and produced PDGF-C and D. These mononuclear cells are known to play important roles in wound healing and inflammatory disease by producing a variety of growth factors and cytokines [23,24]. In our recent study, these mononuclear cells produced inflammatory cytokines (IL-1α, IL-6, TNF-α, NFκB) (submitted for publication). In the present study, these cells also produced PDGF-C and D. Therefore the activation of PDGF-C and D is coincident with inflammation as well as angiogenesis. These findings suggest that PDGF-C and D are involved in multiple aspects of brain RN.

The present and previous reports have revealed that the differential expression of PDGFs has also been seen in pathological conditions other than RN. In the aortic ring outgrowth assay, PDGF-C mediated significantly increased outgrowth, comparable to the levels mediated by VEGF and PDGF-A and B [25]. The angiogenic activity of PDGF-C in vivo is more potent than that of PDGF-A, AB or B [26]. PDGF-D also has been shown to stimulate

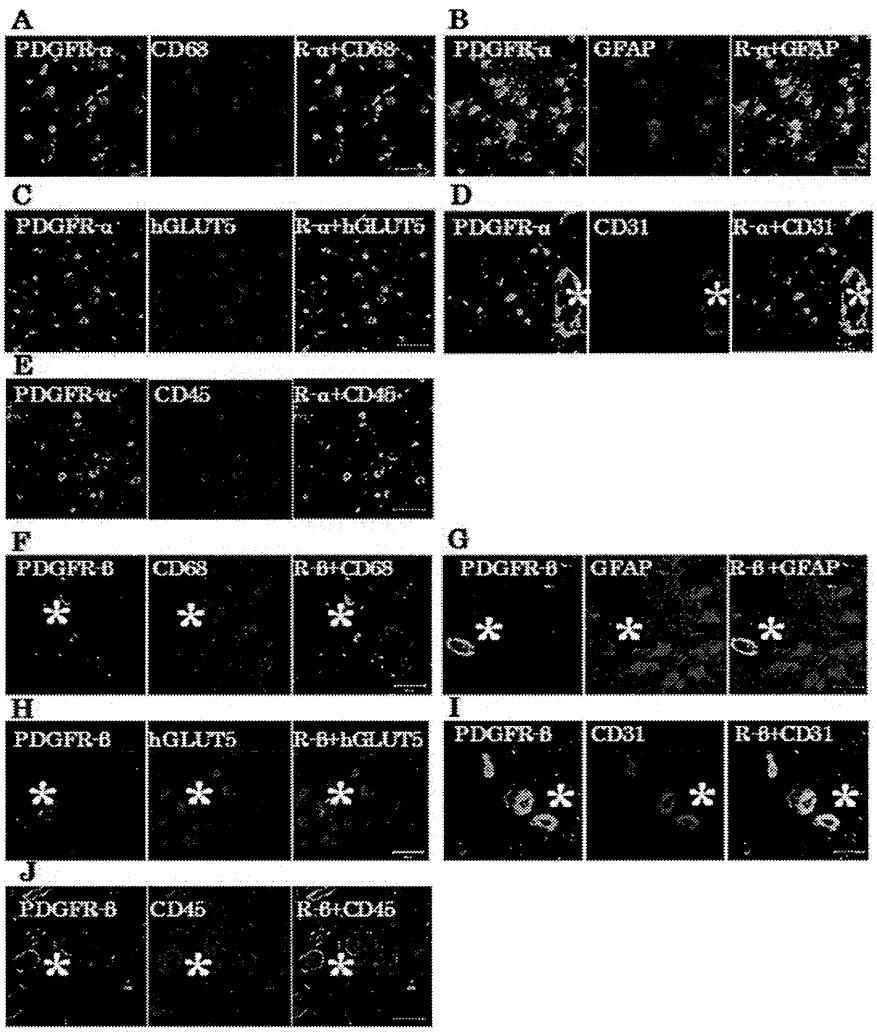

Figure 5 Double immunofluorescence staining. Double immunofluorescence staining from case 1 revealed that PDGFR-α and β were strongly expressed in CD31-positive cells in PN **(D and I)**. PDGFR-α positive cells were merged with many cells positive for CD68 **(A)**, GFAP **(B)**, hGLUT5 **(C)**, and CD45 **(E)**. PDGFR-β-positive cells merged specifically with endothelial cells **(F, G, H, I and J, *)**. Endothelial cells **(*)** were nonspecifically stained with secondary fluorescence antibody. The scale bar represents 50 μm.

angiogenesis and to play a critical role in wound healing [21,27,28].

Li et al. found that PDGF-D is a potent transforming and angiogenic growth factor for NIH/3 T3 cells, and that the transformed cells also induce VEGF expression [28]. Zhao et al. also found that inhibition of PDGF-D leads to decreased cell invasion in gastric cancer, partly through the regulation of VEGF [29]. In our study, many reactive astrocytes produced PDGF-C and D and expressed PDGFR-α, but these cells did not express PDGFR-β. These results established that PDGF-C and D play roles in angiogenesis and inflammation through autocrine and paracrine stimulation. Although the functions of these isoforms of PDGFs on cells are similar in many respects, each isoform might play different roles in different cell types via various receptors and pathways.

Previously, it was reported that several types of cells participate in angiogenesis and inflammation in brain RN [1,5,6]. But the underlying mechanisms have not been completely elucidated. We desperately need to know why different types of cells, including macrophages, microglia, lymphocytes, and astrocytes, acquire the capacity for differentiation, producing inflammatory cytokines and growth factors under certain pathological conditions. Ungvari et al. reported that γ-irradiated cerebromicrovascular endothelial cells acquired a senescence-associated secretory phenotype (SASP) characterized by the upregulation of proinflammatory cytokines and chemokines [30].

Our results suggest that several types of cells that survived irradiation in PN acquired SASP, and that this mechanism may be a key process in brain RN.

In this study, we performed retrospective analysis with clinical specimens of symptomatic RN and revealed that PDGFs/PSGFRs were involved in RN. However, this analysis covers just one aspect of RN. It is impossible to determine whether PDGFs exacerbate RN or rather are produced as a byproduct of RN. Also, we cannot speculate as to the dose–response relationship or the time course of the expression of PDGFs and their receptors in RN. These questions will be answered if a reproducible animal model of RN can be established.

Conclusions

In conclusion, PDGFs/PDGFRs play critical roles in angiogenesis and possibly in inflammation, and they contribute to the pathogenesis of RN, irrespective of the original tumor pathology and applied radiation modality. Moreover, the autocrine or paracrine signaling of PDGFs also plays crucial roles in aggressive angiogenesis and inflammation in RN. PDGF-C, PDGF-D and PDGFR-α have clinical importance, because PDGFR-β was expressed even in UB. Treatments to inhibit PDGF-C and D, or to inhibit PDGF-C and D in combination with PDGFR-α with a kinase inhibitor, may provide new approaches for RN induced by common radiation therapies, including XRT, SRS and BNCT.

Additional files

Additional file 1: Typical MRI of symptomatic radiation necrosis from case 3. Gd-enhanced T1 MRI just prior to excision of necrotic foci (A). Gd-enhanced T1 MRI 2 weeks after surgery (A'). FLAIR MRI just prior to excision of necrotic foci (B). FLAIR MRI, 2 weeks after surgery (B'). After surgical resection of the only enhanced lesion, perilesional edema was decreased compared with preoperative MRI.

Additional file 2: Representative immunohistochemistry from case 1. Immunostaining revealed the necrotic core (A, D NC) and perinecrotic area (A, D PN). PDGF-A (A, B, C) and PDGF-B (D, E) were produced by some monocytic cells (B, E arrow) and endothelial cells (C, E*) in PN. Original magnification, A, D × 40, B, C, E × 200.

Additional file 3: H&E staining and immunohistochemistry from case 3. H&E staining (A) and immunohistochemistry (B through O) from case 3, showing NC and PN. PDGF-A (B, C) and PDGF-B (D, E) were produced by some monocytic cells (arrows in C, E) in PN. In contrast, PDGF-C (F, G, H) and PDGF-D (I, J) were produced by many monocytic cells (arrows in G, H, J), reactive astrocytic cells (arrowheads in G, J), and endothelial cells (H, J*). PDGFR-α (K, L, M) was expressed in monocytic cells (L, arrow), reactive astrocytic cells (L, arrowhead) and endothelial cells (M*) in PN. PDGFR-β (N, O) was expressed mainly in endothelial cells (O*). Original magnification, A, B, D, F, I, K, N × 40, C, E, G, H, J, L, M, O × 200.

Additional file 4: Frequency of expression of PDGFs in the GBM group and non-GBM group. We assessed the frequency of expression of PDGFs semi-quantitatively. In the GBM group (cases 3, 4, 5, 6) and non-GBM group (cases 1, 2, 7), there was no apparent statistical significance in expression of each isoform (A, B, C, D).

Additional file 5: Double immunofluorescence staining results from case 3. Double immunofluorescence staining from case 3 revealed that PDGF-C or D-positive cells were merged with many CD68, hGLUT5, CD45 and GFAP-positive cells. Endothelial cells (*) were nonspecifically stained with secondary fluorescence antibody. The scale bar represents 50 μm.

Additional file 6: Double immunofluorescence staining results from case 3. Double immunofluorescence staining of the specimen from case 3 revealed that PDGFR-α and β were strongly expressed in CD31-positive cells (D and I). PDGFR-α-positive cells were merged with many cells positive for CD68 (A), GFAP (B), hGLUT5 (C), and CD45 (E). PDGFR-β-positive cells were merged specifically with endothelial cells (F thorough J). Endothelial cells (*) were nonspecifically stained with secondary fluorescence antibody. The scale bar represents 50 μm.

Additional file 7: Immunofluorescence staining from consecutive specimens from case 1 and 3. Immunofluorescence staining of consecutive specimens from case 1 (A, B) and 3 (C, D) showed positivity for PDGFR-β (A) or GFAP (B). PDGFR-β (A) was not observable at an excitation wavelength of 561 nm but was apparent at 499 nm in endothelial cells (*). On the other hand, GFAP (B) was observed only at an excitation wavelength of 561 nm in reactive astrocytes. The scale bar represents 50 μm.

Abbreviations

RN: Radiation necrosis; PDGFs: Platelet-derived growth factors; PDGFRs: Platelet-derived growth factor receptors; H&E: Hematoxylin and eosin; PN: Perinecrotic area; UB: Undamaged brain tissue; VEGF: Vascular endothelial growth factor; HIF-1α: Hypoxia-inducible factor 1α; XRT: X-ray treatment; SRS: Stereotactic radiosurgery; Proton: Proton beam therapy; BNCT: Boron neutron capture therapy; NC: Necrotic core; SASP: Senescence-associated secretory phenotype; CTLs: Cytotoxic T-lymphocytes.

Competing interests

The authors declare that they have no competing interests.

Authors' contributions

TM carried out the statistical analysis and drafted the manuscript. S-IM conceived of the study, participated in its design and coordination, and helped to draft the manuscript. TT, NN, MF, HK, EY, SK, and TK participated in the study design and coordination and helped to draft the manuscript. All authors read and approved the final manuscript.

Acknowledgments

This work was partly supported by a Grant-in-Aid for Scientific Research (B) (23390355) and by a Grant-in-Aid for Exploratory Research (24659658) to S-I. M. and by a Grant-in-Aid for Scientific Research (C) (23592145) to M.F. from the Japanese Ministry of Education, Culture, Sports, Science, and Technology. We thank Itsuko Inoue and Kaname Shimokawa for their technical assistance.

Author details

[1]Department of Neurosurgery, Osaka Medical College, 2-7 Daigaku-machi, Takatsuki City, Osaka 569-8686, Japan. [2]Department of Pathology, Osaka Medical College, 2-7 Daigaku-machi, Takatsuki City, Osaka 569-8686, Japan.

Received: 15 October 2013 Accepted: 3 February 2014
Published: 11 February 2014

References

1. Nonoguchi N, Miyatake S, Fukumoto M, Furuse M, Hiramatsu R, Kawabata S, Kuroiwa T, Tsuji M, Ono K: **The distribution of vascular endothelial growth factor-producing cells in clinical radiation necrosis of the brain: pathological consideration of their potential roles.** *J Neurooncol* 2011, 105:423–431.
2. Giglio P, Gilbert MR: **Cerebral radiation necrosis.** *Neurologist* 2003, 9:180–188.
3. Glantz MJ, Burger PC, Friedman AH, Radtke RA, Massey EW, Schold SC Jr: **Treatment of radiation-induced nervous system injury with heparin and warfarin.** *Neurology* 1994, 44:2020–2027.
4. Levin VA, Bidaut L, Hou P, Kumar AJ, Wefel JS, Bekele BN, Grewal J, Prabhu S, Loghin M, Gilbert MR, Jackson EF: **Randomized double-blind placebo-controlled trial of bevacizumab therapy for radiation necrosis of the central nervous system.** *Int J Radiat Oncol Biol Phys* 2011, 79:1487–1495.